島根大学地球科学研究報告　37, 11～19 ページ（2020 年 3 月）
Earth Science Rept. Shimane Univ., 37, p.11～19（2020）

Article

Petrology and geochemistry of pyroclastic rocks from the Masumizuhara pyroclastic flow deposit

Haruna Nishita*, Andreas Auer*

Abstract

Daisen Volcano is located in the San-in district, southwest Japan. The volcano is a large composite cone with several amalgamated eruptive centres which are Hiruzen, Karasugasen, and Misen. A thick apron of pyroclastic material surrounds the entire volcanic complex. The erupted material from Daisen volcano is divided into an Older group and a Younger group. The Masumizuhara pyroclastic flow deposits are sourced from the Misen lava dome and are part of the Younger group. Pyroclastic rocks were analysed by X-ray fluorescence spectrometry (XRF) and all samples are classified as adakitic, medium-K dacites. Mineral and glass composition was determined by electron probe microanalyzer (EPMA) to evaluate magma storage conditions and to characterize the magmatic system of Mt. Daisen during its youngest eruptive cycle. Pressure, temperature, water content and oxygen fugacity range from 126 to 201 MPa, 843 to 864 ˚C, 5.0 to 7.7 wt % and +1.6 to +2.0 log units above the nickel-nickel oxide (NNO) buffer, respectively.

Key words: Daisen Volcano, Misen Lava Dome, Masumizuhara Block and Ash flows, Thermobarometry

Introduction

The physical and chemical properties of magma storage systems are of fundamental importance for understanding magma differentiation, eruption prediction and assessing hazard potential of individual volcanoes (Nakagawa *et al*., 1999). Erupted products contain clues to the magma history, from differentiation in the deep crust to eruption at the surface (Humphreys *et al*., 2006; Auer *et al*., 2015, 2018). This report presents whole rock geochemistry as well as matrix glass and mineral composition of juvenile material from the Masumizuhara pyroclastic flow deposits in order to characterize the magmatic system of Daisen volcano during its youngest eruptive cycle.

Geological Background

Mount Daisen is a large Quaternary stratovolcano located in the San-in district in southwest Japan, and consists of several amalgamated eruptive centers which are: Hiruzen, Karasugasen and Misen. Volcanism in the south-western Japanese arc is related to subduction of the young Philippine Sea Plate and the majority of magmas, erupted from Daisen volcano, have adakitic geochemical characteristics (Morris 1995; Feineman *et al*., 2013; Pineda-Velasco *et al*., 2018; Yamamoto and Hoang 2019). Evolution of the Daisen volcanic complex began during the middle Pleistocene and continued until circa 17,000 years ago and is divided into an Older Group and a Younger Group (Tsukui 1984, 1985). The activity of the Older Group lasted from 1.0 to 0.4 Ma and erupted several thick lava flows in conjunction with depositing the voluminous Mizoguchi tuff breccia. The Older Group is covered by the Younger Group, which is subdivided into an Upper Tephra Group and a Lower Tephra Group. The Younger Group consists of a large number of pyroclastic fall and flow deposits. The last effusive activity of Daisen volcano produced three successive lava domes, which are Karasugasen, Sankoho and Misen all of which produced also large successions of pyroclastic flows (Yamamoto 2017).

Tsukui (1985) suggested that the Misen pyroclastic flows were derived from the Misen lava dome and had been deposited by a relatively active injection at about 17,000 years ago. However, Yamamoto (2017) suggests that the Misen pyroclastic flows were deposited at 28.6 ka and renamed the “Misen” pyroclastic flow deposits into “Masumizuhara” pyroclastic flow deposits. In addition, Tsukui (1984) concluded that the youngest dome forming episode of Daisen volcano produced the Misen lava dome. Yamamoto (2017) introduced an updated stratigraphy in which the Amidagawa pyroclastic flow deposits (20.8 ka), sourced from the Sankoho lava dome, are the most recent eruptive episode. He also provides new 14C age for the Masumizuhara pyroclastic flow of approximately 28.6 ka. We confirmed this updated stratigraphy with a new 14C age collected at Loc.4 (Fig. 1). The analysis was done by radiocarbon dating at AIST, Tsukuba, with a result of 23.4 ka. The Masumizuhara deposits are build up by a large number of Block and Ash flow, occasionally interbedded with more pumice rich layers, presumed to originate from eruption column collapse, which mainly inundated the western flank of Daisen (Fig. 1).

Methods

Field survey was carried out at Hoki town in April-October 2017 and 2018. Stratigraphic logging was done

* Department of Geoscience, Shimane University; 1060 Nishikawatsu, Matsue, 690-8504, Japan

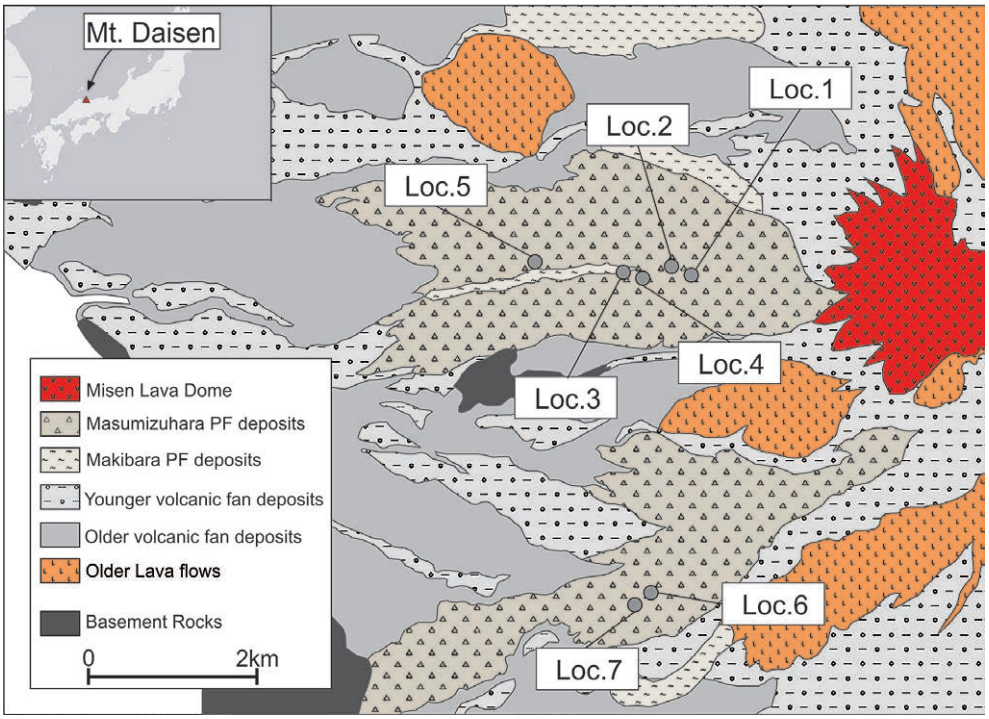

Fig. 1. Geological map of Mt. Daisen simplified after Yamamoto (2017), showing the main distribution of the Masumizuhara pyroclastic flow deposits and their source, the Misen lava dome.

at selected sections and juvenile pyroclastic rocks were collected from each unit. Charcoal, contained in the Masumizuhara pyroclastic flow deposits was analyzed by radiocarbon dating to get the age of last extrusion of the Misen lava dome.

A suite of 5 samples was selected for X-ray fluorescence spectrometry (XRF). All samples were chipped and washed to remove alteration products or weathering rinds. The washed chips were dried at 120 ˚C for 12 hours. The samples were crushed to make powder in a tungsten carbide ring mill with crushing times of 90 seconds. The powder that were put into pots were burned in muffle furnace at 900 ˚C for 2 hours to determine loss on ignition.

Fused glass beads were prepared, using an alkali flux consisting of 80 % lithium tetraborate and 20 % lithium metaborate. The ignited samples of 1.8000 ± 0.0005 g and the flux of 3.6000 ± 0.0005 g were mixed and put into a platinum pot. The glass beads analyzed, using an automatic bead sampler on a Rigaku Co. Ltd. RIX-2000 spectrometer in the Department of Geoscience, Shimane University. Thin sections were prepared for petrography and electron probe microanalyzer (EPMA) investigation. Mineral and glass compositions were analyzed using a JEOL 8530F Field emission microprobe at Shimane University. All analyses were performed at 15 kV and 20 nA with a focused (plagioclase, amphibole, orthopyroxene, Fe-Ti oxide) or defocused (matrix-glass, 8-10 μm) beam. Counting times were 10 second for peak and 5 second for background. Analytical quality has been monitored with Smithsonian standard materials.

Results

1 Outcrops

The Masumizuhara pyroclastic flow (MsP) deposits are exposed on the western and southwestern flank of Daisen volcano. Most outcrop sections are seen along the Seiyama river and the Shirami river. The representative locations of outcrops are shown in Fig. 1. MsP is mainly build up by extensive successions of block and ash flow deposits which include large blocks with low vesicularity and characteristic porphyritic textures (Fig. 2).

2 Whole rock and glass compositions

Major and trace element compositions were determined for vesicle rich samples from pumice flow deposits and porphyritic rocks from block and ash flow deposits (Table 1). The whole rock composition of the Masumizuhara pyroclastic flow deposits have an SiO_2 content ranging from 63 to 65 wt %. All data plot in the dacite field (Fig. 3a) of the total alkali – silica diagram (TAS). The samples taken from the Masumizuhara pyroclastic flow deposits are also classified as adakites (Fig. 3b). Negative correlation with SiO_2 are seen in Al_2O_3, TiO_2, Fe_2O_3 and CaO (Fig. 3c, d, e, f).

All matrix-glass compositions are plotted in rhyolite field (Fig. 3-a).

3 Mineral compositions

The samples collected from block and ash flow deposits are hypocrystalline rocks. The materials are highly porphyritic with low vesicularity and contain large phenocrysts of

Table 1. Matrix-glass and whole rock compositions.

	Matrix-glass			Whole-rock*				
	17102603	17042701	17042702	17042701	17042702	171017MsP1	17102603	Miz1
Oxide								
SiO_2	75.31	75.10	73.35	64.17	63.63	63.46	63.72	64.95
TiO_2	0.28	0.25	0.15	0.43	0.44	0.45	0.42	0.41
Al_2O_3	11.55	12.36	13.29	17.91	18.56	18.48	18.24	17.70
Fe_2O_3	-	-	-	4.12	4.09	4.25	4.02	3.77
FeO	1.16	1.22	0.97	-	-	-	-	-
MnO	0.05	0.01	0.04	0.07	0.07	0.07	0.07	0.07
MgO	0.19	0.13	0.18	1.96	1.84	2.06	1.96	1.73
CaO	0.59	0.86	1.26	4.92	4.91	5.03	5.20	4.78
Na_2O	2.81	3.09	3.57	4.41	4.47	4.35	4.45	4.49
K_2O	3.92	3.60	3.44	1.87	1.80	1.70	1.78	1.98
P_2O_5	-	-	-	0.14	0.20	0.14	0.14	0.14
total	95.85	96.62	96.26	100.00	100.00	100.00	100.00	100.00
Ba				429	479	441	411	458
Ce				35	38	35	36	37
Cr				21	16	20	13	14
Ga				20	21	20	20	19
Nb				6	7	6	6	7
Ni				8	10	9	9	10
Pb				9	11	7	8	10
Rb				49	46	39	46	53
Sr				695	749	712	732	729
Th				4	6	4	3	5
V				58	64	67	56	54
Y				10	11	10	10	10
Zr				121	133	122	118	132

* anhydrous parts normalized to 100

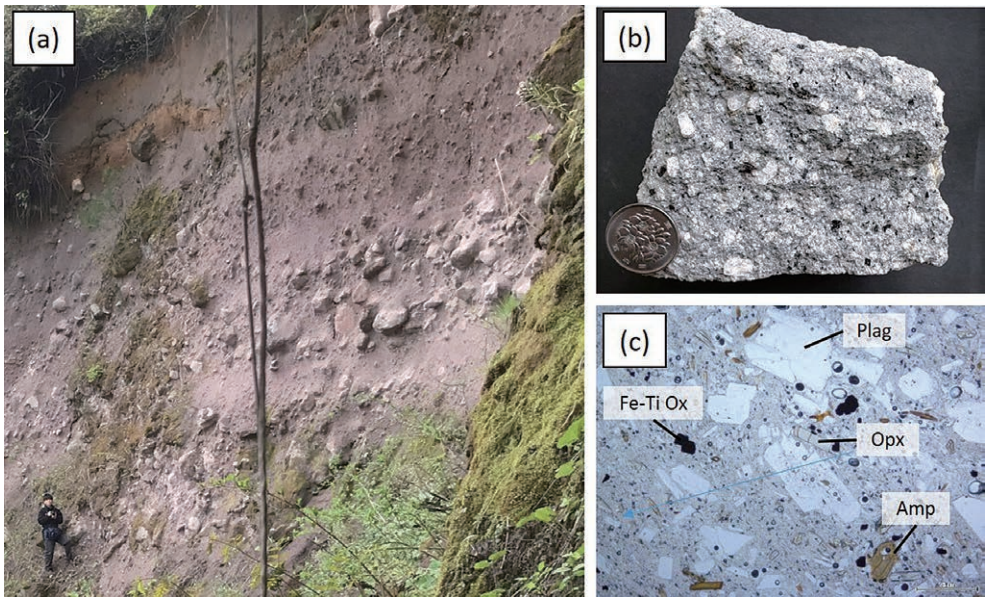

Fig. 2. Representative outcrop of the Masumizuhara pyroclastic flow deposits. (a) Outcrop at Loc. 3 consisted of several deposits from block and ash flows. (b) A hand specimen, showing a porphyritic dacite sample, with abundant plagioclase, from the outcrop at Loc. 3. (c) Thin section image, from a porphyritic sample containing plagioclase, amphibole, orthopyroxene and Fe-Ti oxides.

plagioclase, amphibole, orthopyroxene, Fe-Ti oxide and rarely biotite.

Plagioclase

Plagioclase is the volumetrically dominant phenocryst and groundmass phase in all samples. The modal proportion of plagioclase varies between 11 to 23 %. The maximum crystal length of plagioclase is 3.5-7 mm. Oscillatory zoning is common in most plagioclase crystals (Fig. 4a, b). Plagioclase phenocrysts sometimes have fluid inclusion trails tracing individual zones. The phenocryst core compositions ranges from An 34 to An 38 except for the data of plagioclase which have a sieve-like texture, whereas the groundmass core compositions ranges from An 49 to An 66.

Amphibole

Amphibole is ubiquitous in all samples with euhedral crystals up to 4 mm in size. The modal proportion of

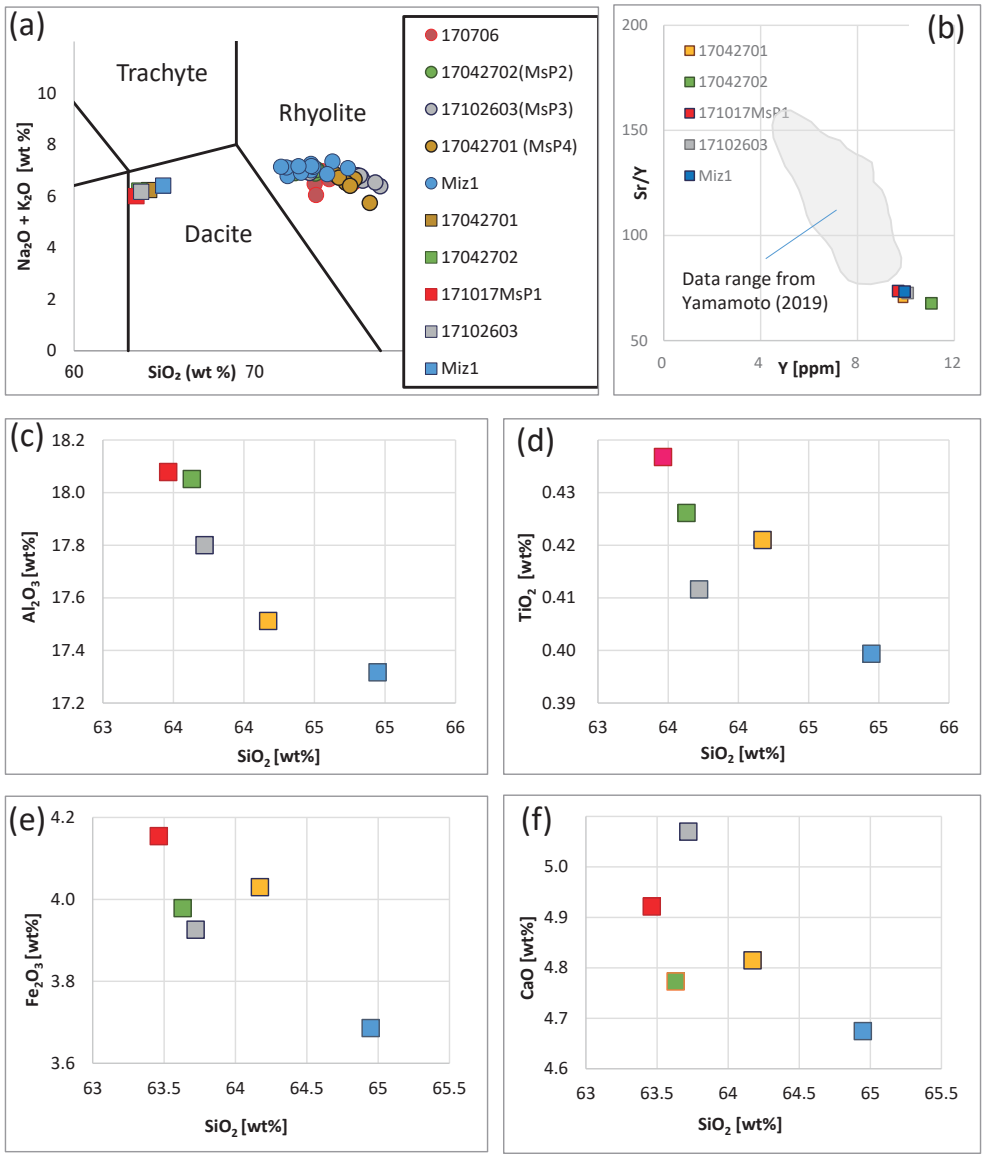

Fig. 3. Geochemical variation diagrams. (a) TAS diagram plotted matrix-glass and whole rock compositions. The circles show the data of matrix-glass and the squares show the data of whole rock composition. (b) Sr/Y vs Y diagram. The grey field shows the data of Yamamoto (2019). (c) Al_2O_3 vs SiO_2 diagram. (d) TiO_2 vs SiO_2 diagram. (e) Fe_2O_3 vs SiO_2 diagram. (f) CaO vs SiO_2 diagram.

amphibole varies between 2.4 to 3.0 %. Amphibole shows strong pleochroism from straw yellow to green. Some amphibole crystals form glomeroporphyritic aggregates with plagioclase and orthopyroxene. Amphibole phenocrysts occasionally enclose biotite. Most amphiboles have sharp edges without breakdown rims (Fig. 4c, d). Amphiboles are classified as tschermakite and magnesio-hornblende after the classification of Leake *et al*. (1997). Some amphiboles show compositional rims of cummingtonite (Fig. 4f). Some representative amphibole analysis are shown in Table 2.

Orthopyroxene

Orthopyroxene occurs as euhedral phenocrysts with sizes up to 1 mm and light pleochroism from light pink to light bluish green. Orthopyroxene hosts Fe-Ti oxides in many samples. The modal proportion of orthopyroxene varies between 2.1 to 2.3 %. The composition of orthopyroxene varies from En64 to En69. Orthopyroxene crystals in the sample of pumice are homogeneous (Fig. 4g), but show compositional zoning in the porphyritic samples. Magnesium numbers range from 0.66 to 0.73. Some representative analysis are shown in Table 2.

Fe-Ti Oxide

Iron – titanium oxides are observed in all samples, They occur as euhedral to subhedral crystals with sizes up to 0.5 mm, often hosted by orthopyroxene. Composition of coexisting magnetite – ilmenite has been determined from intergrown / touching pairs (Fig. 4-f) and some representative analysis are shown in Table 2.

Biotite

Biotite is scarce and often enclosed by amphibole or

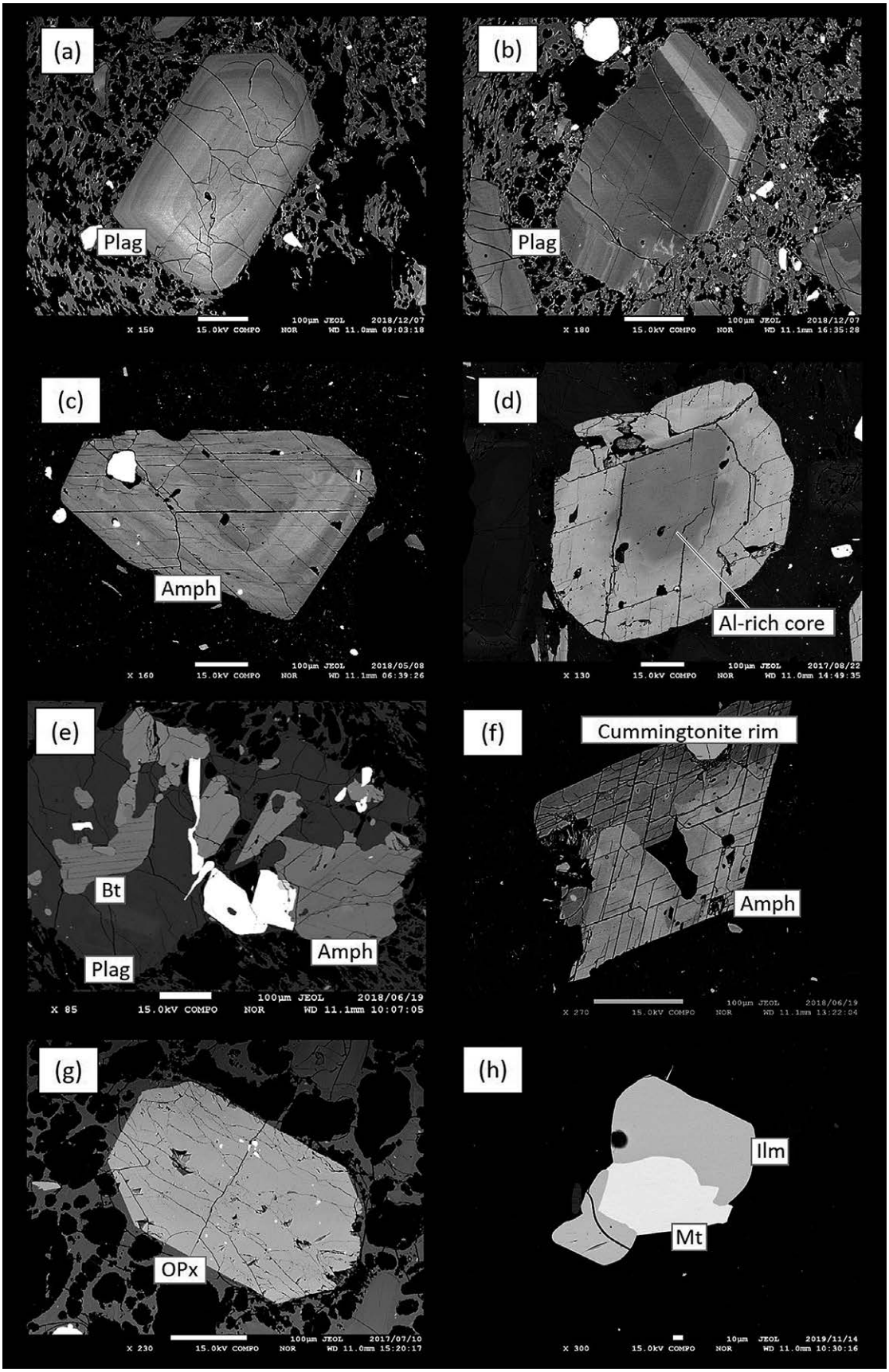

Fig. 4. Backscattered electron images. (a) Plagioclase with oscillatory zoning. (b) Oscillatory zoned plagioclase with Ca rich rim (c) Amphibole with zoning and Mg rich rim. (d) Amphibole with Al-rich core (e) glomeroporphyritic aggregate of Al-rich amphibole and plagioclase, hosting biotite (f) Amphibole with cummingtonite rim (g) Orthopyroxene with no compositional zoning. (h) Co-existing magnetite and ilmenite.

Table 2. Representative mineral compositions.

	Plagioclase		Orthopyroxene			Amphibole		Fe-Ti oxide	
	Miz1-2	Miz1-2	17042702	17042702		Miz1-1	Miz1-1	Miz1-2	Miz1-2
Oxide	7-1	7-2	1-1	1-2		18	19	1-1	1-2
SiO_2	55.56	53.29	53.80	53.57		49.14	45.87	0.06	0.05
TiO_2	0.02	0.04	0.05	0.08		0.85	1.43	5.15	32.29
Al_2O_3	28.31	29.93	0.68	0.92		8.09	10.85	2.16	0.34
Cr2O3	-	-	-	-		-	-	0.09	0.03
FeO	0.12	0.18	21.47	21.64		12.74	13.71	84.99	60.51
MnO	0.02	0.04	0.73	0.74		0.31	0.34	0.31	0.22
MgO	0.00	0.00	24.07	24.04		15.51	13.97	1.31	1.68
CaO	9.95	11.68	0.39	0.38		11.07	10.76	0.00	0.00
Na_2O	5.38	4.56	0.02	0.01		1.27	1.71		
K_2O	0.20	0.16	0.01	0.01		0.32	0.28		
ZnO	-	-	-	-		-	-	0.07	0.00
total	99.57	99.88	101.21	101.39		99.29	98.92	94.15	95.12
Cations (O)	**8**	**8**	**6**	**6**		**22**	**22**	**32**	**6**
Si	2.51	2.41	1.97	1.96		6.84	6.46	0.02	0.00
Ti	0.00	0.00	0.00	0.00		0.09	0.15	1.16	1.25
Al	1.51	1.60	0.03	0.04		1.33	1.80	0.77	0.02
Cr	-	-	-	-		-	-	0.02	0.00
Fe^{3+}	-	-	-	-		1.10	1.21	12.85	1.48
Fe^{2+}	0.00	0.01	0.66	0.66		0.38	0.40	8.50	1.11
Mn	0.00	0.00	0.02	0.02		0.04	0.04	0.08	0.01
Mg	0.00	0.00	1.31	1.31		3.22	2.93	0.59	0.13
Ca	0.48	0.57	0.02	0.01		1.65	1.62	0.00	0.00
Na	0.47	0.40	0.00	0.00		0.34	0.47		
K	0.01	0.01	0.00	0.00		0.06	0.05		
Zn	-	-	-	-		-	-	0.02	0.00
total	4.98	4.99	4.01	4.02		15.05	15.14	24.00	4.00
An	50.0	58.1	*Mg#*	0.7	0.7	*Mg#*	0.89	0.88		
Ab	48.8	41.0	*Wo*	0.8	0.7					
Or	1.2	1.0	*En*	65.5	65.3					
			Fs	33.8	34.0					

Mg# = Mg / ($Mg+Fe^{2+}$)

plagioclase phenocrysts (Fig. 4e). The modal proportion of biotite is 0.3 to 0.5 %. Biotite shows a platy habit and typical mottled extinction. Brown biotite is observed and it suggests that the brown crystals may have been formed by the oxidation during and after the eruption (Tsukui 1985).

Discussion

Magma temperature and Pressure

Magma temperature and pressure were estimated using amphibole thermobarometry (Ridolfi *et al*., 2010) and orthopyroxene thermobarometry (Putirka 2008). Additional constrain for magmatic temperatures comes from Fe-Ti-oxide thermometry (Lepage 2003). Temperature estimates using the Ridolfi *et al*. (2010) model for over 100 amphiboles and the Putirka (2008) model for 37 orthopyroxene analyses are shown in Fig. 5a. The pressure-temperature (P-T) estimates from amphibole show a range of 105 to 432 MPa and 797 to 953 ˚C. The majority of amphiboles clusters at or below 200 MPa. For some amphiboles, significantly higher pressures were obtained, for example for Al-rich cores (Fig. 4d) or for amphiboles within glomeroporphyritic aggregates. The P-T estimates for orthopyroxene varies from 0 to 201 MPa and 843 to 858 ˚C. The temperature estimates using the ILMAT model of Lepage (2003) for Fe-Ti oxide analysis show a range 847 to 886 ˚C (Fig. 5-c). The overlapping range from all three models lies between 126 to 201 MPa and 843 to 864 ˚C and is assumed to reflect the main pressure and temperature range of shallow magma storage at Mt Daisen for the Masumizuhara eruptions, corresponding to a crustal depth between 4.8 km and 7.6 km. The presence of cummingtonite rims on some amphiboles is in agreement with our results because cummingtonite is indicative of voluminous, shallow magma chambers below 4 kbar and H_2O-rich magmas close to or at saturation (Evans and Ghiorso 1995).

Oxygen fugacity

Oxygen fugacity was calculated using the Ridolfi *et al*. (2010) model and the ILMAT model of Lepage (2003). Oxygen fugacity estimates using the Ridolfi *et al*. (2010) model for amphibole analysis ranges from +0.5 to NNO+2.3 log units above the nickel-nickel oxide (NNO) buffer (Fig. 5c). Oxygen fugacity estimates using the ILMAT model of Lepage (2003) for Fe-Ti oxide analysis ranges from +1.6 to NNO+2.0 log units above the NNO mineral buffer.

Water content

Magma water contents were calculated based on the plagioclase-liquid hygrometer of Lange *et al*. (2009) and the Ridolfi *et al*. (2010) model. The water content estimated using the Ridolfi *et al*. (2010) model for amphibole varies from 5.0 to 7.8 wt % (Fig. 5-b). The water content calculated using the plagioclase-liquid hygrometer of Lange *et al*. (2009) assuming average glass and plagioclase compositions together with temperature and pressure estimates from the amphibole geothermobarometer ranges from 4.0 to 7.7 wt %. The overlapping range between 5.0 to 7.7 wt % is the presumed water content of the dacitic magmas from Daisen during its youngest episode of activity.

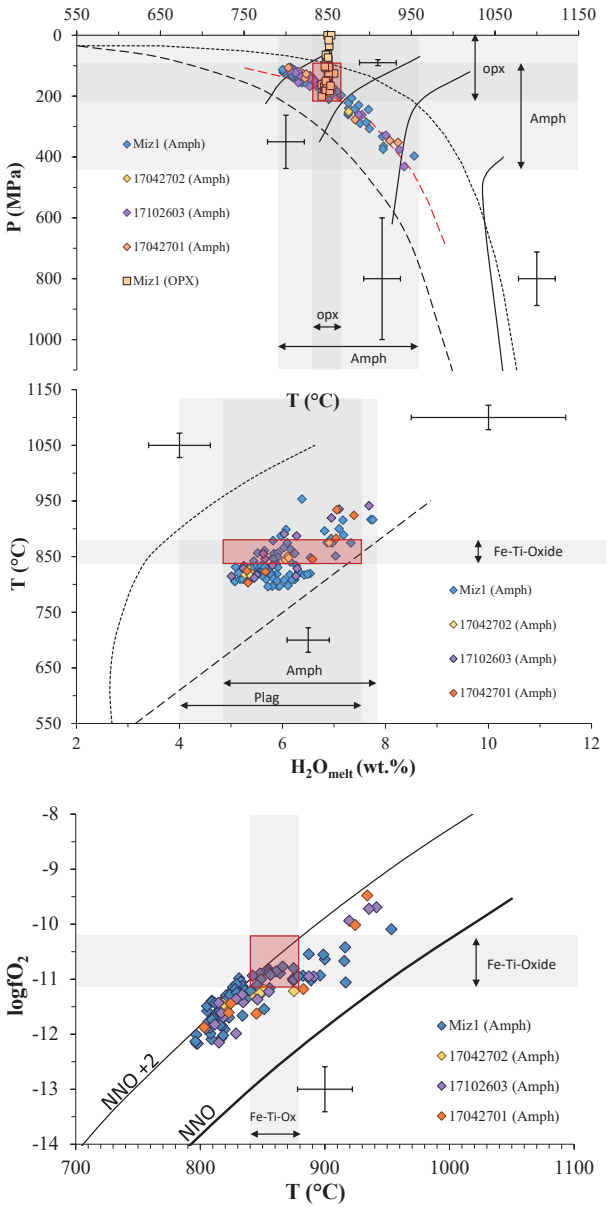

Fig. 5. (a) P-T diagram, showing crystallization conditions using amphibole composition (diamond shapes) after Ridolfi *et al*. (2010) and orthopyroxene (square shapes) after Putirka *et al*. (2008). The red area shows overlapping conditions from both thermobarometers, presumed to represent the main shallow storage of magma beneath Mt. Daisen. (b) T - H_2O melt diagram plotted the data of amphibole, orthopyroxene and plagioclase. (c) log fO_2-T diagram based on the amphibole and Fe-Ti oxide data.

Conclusion

All samples from the Masumizuhara pyroclastic flow

deposits are classified as adacitic, medium-K dacites. All matrix-glass compositions plot in the rhyolite field of the TAS diagram. Materials contain large phenocrysts of plagioclase, amphibole, orthopyroxene, Fe-Ti oxide, and rarely biotite. The temperature, pressure and water content are estimated from these minerals using different established models. We determined pressure (Amph, OPx), temperature (Amph, OPx, Fe-Ti – oxide), oxygen fugacity (Amph, Fe-Ti - oxide) and water content (Amph, Plag) for our samples using at least two independent methods. Our final estimates are derived from the overlapping range for all physical conditions. In the pressure-temperature diagram (Fig. 5a) the data of amphibole and orthopyroxene shows an overlapping range of temperature between 843 and 864 ˚C and pressure varies from 126 to 201 MPa. In the water content diagram, the overlapping range of water content varies from 5.0 to 7.7 wt %. In the oxygen fugacity diagram the range of oxygen fugacity varies from +1.6 to +2.0 log units above NNO. These values are interpreted as the main shallow storage conditions of magma during the Masumizuhara eruptions.

Acknowledgement

We would like to thank Takahiro Yamamoto who is a researcher of AIST for support in the field and also for helping us with radiocarbon dating of the charcoal samples.

References

Auer A, Belousov A, Belousova M (2018) Deposits, petrology and mechanism of the 2010–2013 eruption of Kizimen volcano in Kamchatka, Russia. *Bull Volcanol*, **80**, 33.

Auer A, Martin CE, Palin JM, *et al*. (2015) The evolution of hydrous magmas in the Tongariro Volcanic Centre: the 10 ka Pahoka-Mangamate eruptions. *N Z J Geol Geophys*, **58**, 364–384. https://doi.org/10.1080/00288306.2015.1089913

Evans BW, Ghiorso MS (1995) Thermodynamics and petrology of cummingtonite. *Am Mineral*, **80**, 649–663.

Feineman M, Moriguti T, Yokoyama T, *et al*. (2013) Sediment-enriched adakitic magmas from the Daisen volcanic field, Southwest Japan. *Geochem Geophys Geosystems*, **14**, 3009–3031.

Humphreys MCS, Blundy JD, Sparks RSJ (2006) Magma evolution and open-system processes at Shiveluch Volcano: Insights from phenocryst zoning. *J Petrol*, **47**, 2303–2334. https://doi.org/10.1093/petrology/egl045

Lange RA, Frey HM, Hector J (2009) A thermodynamic model for the plagioclase-liquid hygrometer/thermometer. *Am Mineral*, **94**, 494–506. https://doi.org/10.2138/am.2009.3011

Leake BE, Woolley AR, Arps CE, *et al*. (1997) Report. Nomenclature of Amphiboles: Report of the Subcommittee on Amphiboles of the International Mineralogical Association Commission on New Minerals and Mineral Names. *Mineral Mag*, **61**, 295–321.

Lepage LD (2003) ILMAT: an Excel worksheet for ilmenite–magnetite geothermometry and geobarometry. *Comput Geosci*, **29**, 673–678.

Morris PA (1995) Slab melting as an explanation of Quaternary volcanism and aseismicity in southwest Japan. *Geology*, **23**, 395–398. https://doi.org/10.1130/0091-7613(1995)023<0395:SMAAEO>2.3.CO;2

Nakagawa M, Wada K, Thordarson T, *et al*. (1999) Petrologic investigations of the 1995 and 1996 eruptions of Ruapehu volcano, New Zealand: formation of discrete and small magma pockets and their intermittent discharge. *Bull Volcanol*, **61**, 15–31.

Pineda-Velasco I, Kitagawa H, Nguyen T-T, *et al*. (2018) Production of high-Sr andesite and dacite magmas by melting of subducting oceanic lithosphere at propagating slab tears. *J Geophys Res Solid Earth*, **123**, 3698–3728.

Putirka KD (2008) Thermometers and Barometers for Volcanic Systems. In: Putirka KD, Tepley FJ (eds) Minerals, Inclusions and Volcanic Processes. *Mineralogical Soc Amer, Chantilly*, pp 61–120.

Ridolfi F, Renzulli A, Puerini M (2010) Stability and chemical equilibrium of amphibole in calc-alkaline magmas: an overview, new thermobarometric formulations and application to subduction-related volcanoes. *Contrib Mineral Petrol*, **160**, 45–66. https://doi.org/10.1007/s00410-009-0465-7

Tsukui M (1984) Geology of Daisen Volcano. *J Geol Soc Jpn*, **90**, 643–658. https://doi.org/10.5575/geosoc.90.643

Tsukui M (1985) Temporal variation in chemical composition of phenocrysts and magmatic temperature at Daisen volcano, southwest Japan. *J Volcanol Geotherm Res*., **26**, 317–336.

Yamamoto T (2017) Quantitative eruption history of Pleistocene Daisen volcano, SW Japan. *Bull Geol Surv Jpn*, **68**, 1–16.

Yamamoto T, Hoang N (2019) Geochemical variations of the Quaternary Daisen adakites, Southwest Japan, controlled by magma production rate. Lithos 350:105214.

(Received: Feb. 20, 2020, Accepted: Feb. 28, 2020)

（要　旨）

西田華菜・Andreas Auer，2020．桝水原火砕流堆積物における岩石学的および地球化学的研究．島根大学地球科学研究報告，37，11-19

大山火山は西日本の山陰地方に位置している．また，蒜山，烏ヶ山，弥山といった噴火口を持つ巨大な複合火山であり，全体的に厚い火山噴出物で覆われている．大山火山の噴出物は主に，新期噴出物と古期噴出物に分けることができ，弥山溶岩ドーム起源である桝水原火砕流堆積物は新期噴出物に分類される．本研究では，電子マイクロプローブアナライザーと蛍光 X 線分析装置を用いて，鉱物およびガラスの組成を分析し，大山火山の活動最終期の浅部マグマだまりの温度，圧力，含水量そして酸素フガシティーを推定した．結果として，温度，圧力，含水量および酸素フガシティーはそれぞれ，843~864 ˚C, 126-201 MPa, 5.0-7.7 wt%, nickel-nickel oxide (NNO) buffer +1.6~NNO+2.0 log unit となった．